# *Pn* arrivals and lateral variations of Moho geometry beneath the Kaapvaal craton

M.T.O.G. Kwadiba[a,b], C. Wright[a,*], E.M. Kgaswane[a,1], R.E. Simon[a,c], T.K. Nguuri[a,2]

[a] *Bernard Price Institute of Geophysical Research, School of Earth Sciences, University of the Witwatersrand, Johannesburg, Private Bag 3, Wits 2050, South Africa*

[b] *Geophysics Division, Department of Geological Survey, Private Bag 14, Lobatse, Botswana*

[c] *Department of Physics, University of Botswana, Private Bag UB707, Gaborone, Botswana*

**Abstract**

*Pn* arrivals from mining-induced earthquakes on the edge of the Witwatersrand basin show that the P wavespeeds in the uppermost mantle are almost constant throughout most of the Kaapvaal craton. The presence of only small wavespeed variations allows the use of a simple method of estimating crustal thicknesses below the stations of the Kaapvaal broad-band network using *Pn* times that has been compared with results from receiver functions. One thousand three hundred thirty-seven *Pn* arrivals were used to derive crustal thicknesses at 46 stations on the Kaapvaal craton. The average crustal thicknesses for 19 centrally located stations on each of the northern and southern regions of the craton that yielded well-constrained thicknesses were $50.52 \pm 0.88$ km and $38.07 \pm 0.85$ km, respectively. In contrast, the corresponding average thicknesses determined from receiver functions were $43.58 \pm 0.57$ km and $37.58 \pm 0.70$ km, respectively. The systematically lower values for receiver functions in the northern part of the Kaapvaal craton that was affected by the Bushveld magmatism at 2.05 Ga, suggest that the receiver functions do not enable the petrological crust mantle boundary to be reliably resolved due to variations in composition and metamorphic grade in a mafic lower crust. The *Pn* times also suggest pervasive azimuthal anisotropy with maximum wavespeeds of about 8.40 km/s at azimuths of about 15° and 217° in the northern and southern regions of the craton, respectively, and minimum wavespeeds of about 8.25 km/s.



*Keywords:* Crustal thickness; Kaapvaal craton; Mining-induced earthquakes; *Pn* arrivals; Properties of lower crust

## 1. Introduction

Southern Africa comprises a large continental craton of Precambrian age with moderate seismic activity (Kulhanek and Meyer, 1979). Most of the earthquakes in the southern part of the continent are associated with the East African Rift, which is characterized by extensional tectonics (Kulhanek and Meyer, 1979). South Africa lies in this intraplate region, which is situated thousands of kilometres away from the seismically active mid-oceanic ridges in the south Atlantic and in the southwest Indian ocean (Andreoli et al., 1996). Few tectonic events occur within South Africa, and most seismic events

* Corresponding author. Fax: +27-11-717-6579.

*E-mail address:* wrightc@geosciences.wits.ac.za (C. Wright).

[1] Present address: Council for Geoscience, Private Bag X112, Pretoria 0001, South Africa.

[2] Present address: PREPCOM CTBTO,Vienna International Centre, P.O. Box 1250, A-1400, Vienna, Austria.

located within the country are related to gold mining in the Witwatersrand basin. These mining-induced events have been used to determine the structure of the crust and upper mantle in the central regions of the Kaapvaal craton, and earlier work was summarised by Wright and Fernandez (2003) and Wright et al. (2002, 2003). The Southern African Broadband Seismic experiment (SABSE) provided the opportunity to better define South African seismicity over a 2-year period. A database of waveforms recorded during the SABSE, which consists mainly of mining-induced events, was assembled (Kgaswane et al., 2002; Wright et al., 2003), and provided the data used in this paper.

Receiver functions provide another approach to measuring crustal thicknesses that was used to show that the crust beneath the southern region of the Kaapvaal craton that has remained undisturbed since the Archaean has a simple crust–mantle transition at depths typically between 35 and 40 km. In contrast, the adjacent Proterozoic mobile belts exhibit complex Moho signatures and thicknesses of 45 to 50 km (Nguuri et al., 2001). The northern parts of the Kaapvaal craton around the Bushveld complex, however, show receiver functions that indicate more complicated crust–mantle transitions that exhibit similar character to those in the adjacent mobile belts.

The objective of the present study is to define variations in crustal thicknesses beneath the Kaapvaal craton using *Pn* arrivals recorded at those SABSE stations located within the craton or very close to the craton margin. Comparison of our results with those from receiver functions (Nguuri et al., 2001) has been made to provide complementary information on the structure and properties of the lower crust and uppermost mantle. According to Baumont et al. (2001), *Pn* travel times are sensitive to Moho geometry, the crustal $V_p$, the upper mantle $V_p$ to a lesser extent, and not sensitive to crustal $V_s$. $V_p$ and $V_s$ are the P and S wavespeeds, respectively. The time delays between the P and P-to-S converted arrivals in receiver functions are sensitive to Moho depth, and both the average crustal $V_p$ and $V_s$. The effectiveness of the method also depends primarily on the S wavespeed contrast at the Moho. Therefore, comparison of crustal thicknesses estimated using receiver functions and refracted arrivals will assist in better understanding the seismic properties and petrology of the lower crust (Wright et al., 2003). Furthermore, our results will be used to define starting models for tomographic inversion for the structure of the crust and uppermost mantle of the Kaapvaal craton and surrounding regions. The present work provides the basis for more comprehensive 3-D studies of seismological structure, in which *Pn* times are used to define crustal thicknesses below individual stations of the SABSE. Comments on identification of the reflected phase *PmP* to provide further constraints on crustal thicknesses, and discussion of 'record sections' are also provided.

## 2. General geological setting

The geology of the mine source regions was described by Pretorius (1986). On a larger scale, de Wit et al. (1992) gave an account of the Archaean history of South Africa. Southern Africa comprises a well-defined Archaean continental nucleus surrounded by Proterozoic mobile belts (de Wit et al., 1992; Carlson et al., 1996). The Archaean region (Fig. 1) is made up of the Kaapvaal and Zimbabwe cratons, consisting of low-grade metamorphosed granite–greenstone terrains, welded together by a 250-km wide ENE-trending high-grade tectono-metamorphic terrain of the Limpopo belt (Van Zijl, 1978; de Wit et al., 1992). The high-grade gneisses and granulites constituting the Limpopo belt have been considered to be the ensialic reworking of cratonic material (Mason, 1973). The cratonic regions are bordered to the south by the Namaqua-Natal mobile belt, to the west by the Kheis belt and to the east by the Lebombo monocline (de Wit et al., 1992).

The Kaapvaal craton formed and stabilised between 3.7 and 2.7 Ga (Carlson et al., 1996) and covers an area of $1.2 \times 10^6$ km$^2$ (de Wit et al., 1992); it has been extensively studied because of its great concentration of mineral resources (Boyd et al., 1985; Boyd and Gurney, 1986), but relatively little geophysical work has been done.

The composition of the continental crust is established to be andesitic, which cannot have been produced by the basaltic magmatism that presently

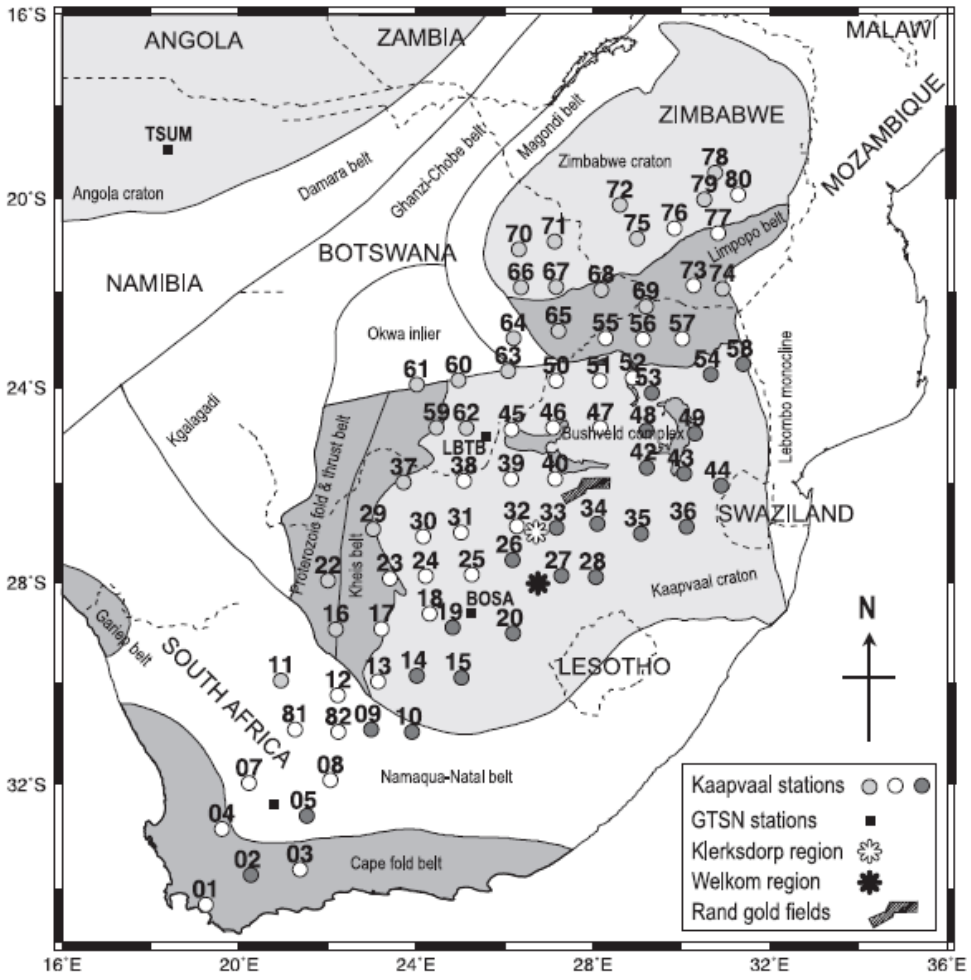


Fig. 1. Map of southern Africa showing distribution of stations of the April 1997–April 1999 Southern African Broadband Seismic Experiment superimposed on the major crustal blocks of southern Africa (After de Wit et al., 1992; Carlson et al., 1996; Nguuri et al., 2001). The grey circles, open circles and dark grey circles denote stations deployed during the period April 1997–April 1998, April 1997–April 1999 and April 1998–April 1999, respectively. The closed squares symbolise the Global Telemetered Seismological Network (GTSN). Locations of the Klerksdorp and Welkom mining regions are shown as open and closed asterisks, respectively.

operates at convergent margins and within plates (Rudnick, 1995). This makes it more difficult to accept that the continental crust is derived by partial melting of the underlying mantle, leaving a highly depleted refractory peridotite (Hofmann, 1988). Furthermore, laboratory-melting experiments carried out on mantle peridotite produce basaltic and picritic magmas (Ireland et al., 1994; Rudnick,

1995). This poses a paradox: if the crust is formed by processes of partial melting at high pressures, why is the crust not basaltic? Seismological investigations provide important clues to the processes of formation that led to the present composition of the continents.

## 3. Sources of data and methodology

The data consist of seismograms from 60 mining-induced tremors recorded by stations of the SABSE: 20 in each of the Far West and West Rand, Klerksdorp and Welkom areas (Fig. 2). Events with local magnitudes greater than 3.0 were used to ensure reasonably strong arrivals to distances of at least 700 km and the locations are shown in Fig. 3. Epicentres were obtained from mine catalogues and converted to latitudes and longitudes relative to the World Geodetic Service, 1984 (WGS84) (Kgaswane et al., 2002). Origin times were derived from the Council for Geoscience earthquake bulletins (Graham, 1997, 1998, 1999) and corrected by the method described by Wright et al. (2003). For time picking of first arrivals (*Pg* or *Pn*), all seismograms were bandpass filtered between 0.4 and 4.0 Hz.

## 4. Determination of crustal thicknesses from *Pn* arrivals

The present data consist of *Pn* arrivals distributed over a wide area (Fig. 1) and differ from those of Baumont et al. (2001) who used approximately linear profiles of broad-band stations to estimate crustal thicknesses. The method of determining crustal thickness is similar in principle to that of Baumont et al., and relies on the result that the upper mantle wavespeed is practically uniform across the entire Kaapvaal craton. Similar studies that use *Pn* arrivals to define Moho topography have been described by Vetter and Minster (1981), Shearer and Oppenheimer (1982) and Zervas and Crosson (1986). A fundamental difficulty with the present data is the concentration of sources in three restricted geographical areas, which does not allow the construction of

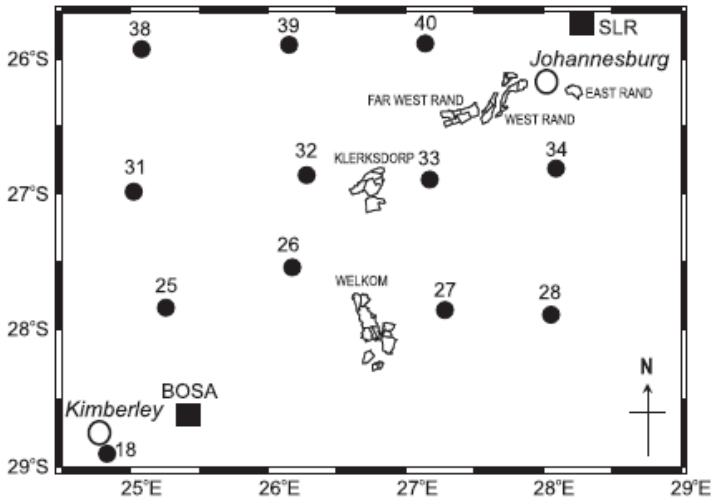


Fig. 2. Location map of the East Rand, West Rand, Far West Rand, Klerksdorp and Welkom source regions in the Witwatersrand basin. Also shown on the map are some of the seismic stations of the SABSE project in Fig. 1 (circles). Squares denote permanent broadband or long-period seismic stations.

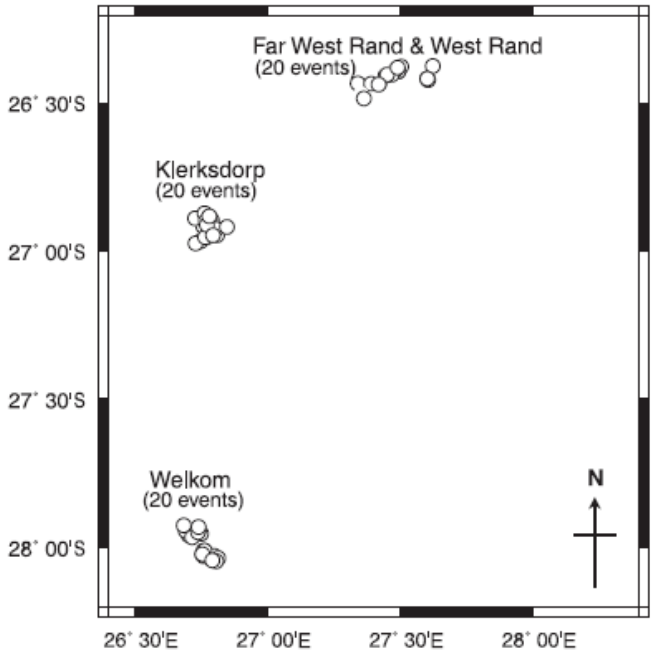


Fig. 3. Location map of the 60 events used as seismic sources in this study. The epicentres are denoted by open circles, which are distributed in clusters around the mining regions as shown on the map. These events generated 1337 *Pn* arrival time picks for stations on the Kaapvaal craton or very close to the craton margin. The names of the source regions are also indicated together with the number of events from each region.

reversed refraction profiles that are commonly used in crustal-scale seismic refraction work. There is also the need to estimate crustal thicknesses at the sources using other data.

Wavespeed models for the crust corresponding to those of Table 2 of Wright et al. (2003) were used in which depth variations were implemented by keeping the wavespeeds constant at 6.80 and 7.10 km/s at 20 km depth and at the base of the crust, respectively, and having a constant wavespeed gradient within that region. In the uppermost mantle, wavespeed models with low positive gradients that give an average ray parameter of 1/8.37 s/km were chosen. Ray tracing was then undertaken through spherically symmetric models with crustal thicknesses at 2 km separations, varying from 36 to 56 km, and the travel–time curves and *Pn* times were superimposed on reduced-time (T-D/8.37) graphs (Fig. 4). For each station, all time observations for the *Pn* phase for a particular source region were plotted interactively on the reduced-time plots, and an average crustal thickness for that source-to-station path estimated for each time value.

Each estimated thickness can be regarded as approximately the average of the crustal thickness beneath the source and the recording station. To obtain a crustal thickness below the station, an assumption has to be made concerning the thickness below the source. Since the average crustal thicknesses estimated from *Pn* arrivals are slightly greater than those estimated from receiver functions, and the thicknesses estimated from receiver functions are slightly larger below and around the Witwatersrand basin than below much of the south-

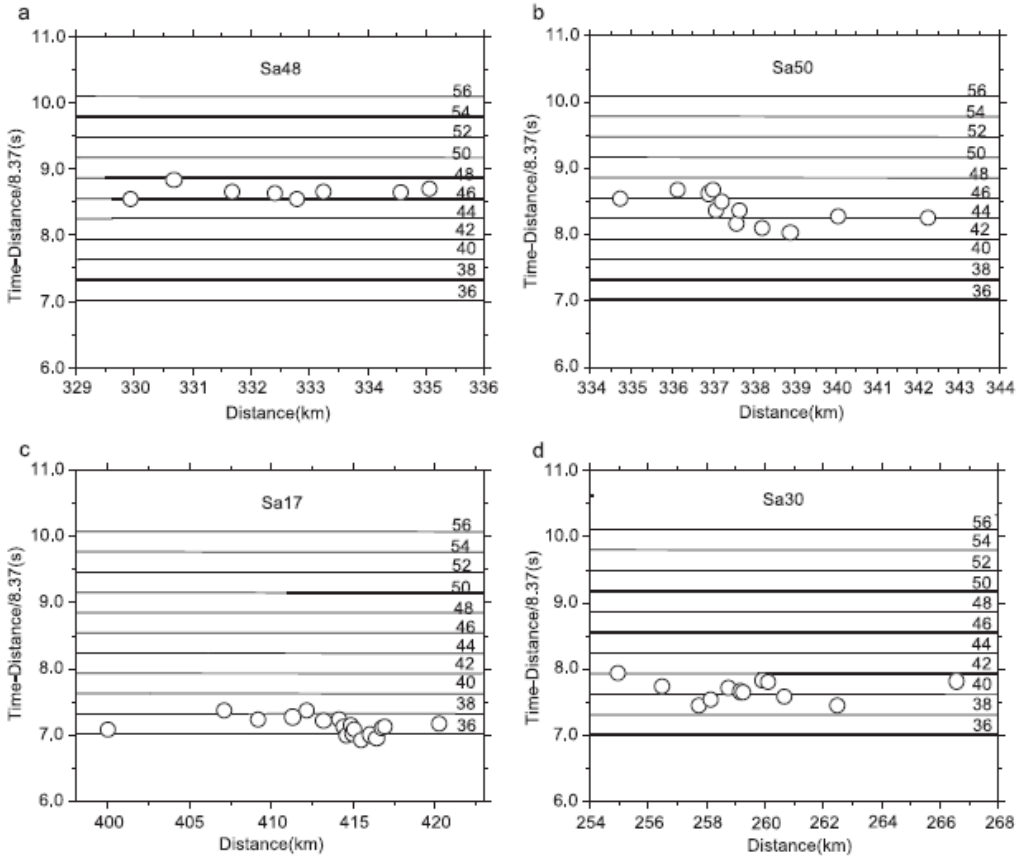


Fig. 4. Reduced travel-time curves from P wavespeed models used in the estimation of average crustal thicknesses. a, b, c and d are examples of plotted *Pn* times against the predicted thicknesses in the background for stations Sa48, Sa50, Sa17 and Sa30, respectively, for 20 events in the Klerksdorp region (Fig. 3).

ern part of the Kaapvaal craton, a starting thickness of 45 km was assumed for events from the Far West and West Rand regions. The average crustal thickness from receiver functions for stations close to this source region was 42 km (Wright et al., 2003).

Notes to Table 1:

[a] Estimates of crustal thicknesses from *Pn* arrivals were determined from one or more source regions: KL—Klerksdorp; WE—Welkom; WR—Far West and West Rand; All—All three source regions.

[b] Stations marked [b] were used to compute averages for comparison of[c] thicknesses from *Pn* arrivals with those from receiver functions. Stations yielding a bimodal distribution of thicknesses from *Pn* times have two entries marked (a) and (b). Stations SA139 and SA155 are stations less than 40 km from SA39 and SA55 respectively; they are not marked as separate stations in Figs. 1 and 7.

Table 1
List of crustal thicknesses based on *Pn* arrival times and receiver function analysis for the southern and northern regions of the Kaapvaal craton

| Station | Mean thickness (km) | Standard error (km) | No. of estimates | Source regions[a] | Receiver function thickness (km) | Difference (km) |
|---|---|---|---|---|---|---|
| *South* | | | | | | |
| BOSA[b] | 38.58 | 0.89 | 36 | KL, WR | 35.0 | 3.6 |
| SA12[b] | 36.63 | 0.64 | 58 | All | 45.0 | −8.4 |
| SA13[b] | 34.29 | 0.54 | 53 | All | 35.0 | −0.7 |
| SA14[b] | 36.47 | 1.03 | 25 | All | 34.0 | 2.5 |
| SA15[b] | 35.20 | 1.57 | 14 | All | 38.0 | −2.8 |
| SA16 | 47.01 | 0.94 | 32 | All | 36.0 | 11.0 |
| SA17[b] | 31.13 | 0.61 | 52 | All | 38.0 | −6.9 |
| SA18[b] | 35.49 | 0.88 | 42 | All | 36.0 | −0.5 |
| SA19[b] | 37.33 | 0.97 | 26 | All | 36.0 | 1.3 |
| SA20[b] | 38.21 | 1.33 | 17 | KL, WR | 38.0 | 0.2 |
| SA22 | 56.49 | 0.77 | 21 | All | 35.0 | 21.5 |
| SA23[b] | 35.08 | 0.81 | 41 | All | 44.0 | −8.9 |
| SA24[b] | 34.16 | 0.85 | 35 | All | 38.0 | −3.8 |
| SA25[b] | 39.15 | 1.25 | 16 | WR | 38.0 | 1.2 |
| SA29[b] | 42.21 | 0.98 | 21 | All | 35.0 | 7.2 |
| SA30[b] | 39.27 | 1.09 | 38 | All | 35.0 | 4.3 |
| SA31[b] | 41.78 | 1.05 | 30 | WE, WR | 40.0 | 1.8 |
| SA35[b] | 37.25 | 1.19 | 10 | KL, WE | 40.0 | −2.8 |
| SA36[b] | 43.10 | 1.43 | 21 | All | 38.0 | 5.1 |
| SA37[b] | 46.46 | 0.96 | 31 | All | 34.0 | 12.5 |
| SA38(a)[b] | 41.50 | 0.89 | 27 | KL, WR | 37.0 | 4.5 |
| SA38(b) | 53.53 | 1.44 | 15 | WE | 37.0 | 16.5 |
| *North* | | | | | | |
| LBTB[b] | 50.95 | 0.60 | 51 | All | 45.0 | 6.0 |
| SA39[b] | 51.97 | 4.96 | 6 | WE | 42.0 | 10.0 |
| SA139[b] | 51.10 | 2.83 | 6 | WE | 40.0 | 11.1 |
| SA40[b] | 40.84 | 0.67 | 20 | WE | 45.0 | −4.2 |
| SA42[b] | 41.42 | 1.05 | 13 | KL, WE | 42.0 | −0.6 |
| SA44[b] | 49.74 | 1.60 | 23 | All | 40.0 | 9.7 |
| SA45[b] | 56.74 | 0.92 | 53 | All | 45.0 | 11.7 |
| SA46[b] | 54.66 | 0.84 | 38 | KL, WE | 44.0 | 10.7 |
| SA47[b] | 51.03 | 0.75 | 29 | KL, WE | 45.0 | 6.0 |
| SA48[b] | 49.87 | 1.02 | 24 | All | 45.0 | 4.9 |
| SA50[b] | 48.94 | 0.72 | 36 | All | 43.0 | 5.9 |
| SA51(a) | 45.00 | 0.79 | 38 | KL, WE | 50.0 | −5.0 |
| SA51(b) | 53.63 | 1.14 | 20 | WR | 50.0 | 3.6 |
| SA53[b] | 51.06 | 1.25 | 13 | All | 43.0 | 8.1 |
| SA54[b] | 50.47 | 2.04 | 7 | KL, WE | 38.0 | 12.5 |
| SA55[b] | 50.68 | 1.19 | 33 | All | 44.0 | 6.7 |
| SA155[b] | 50.87 | 1.48 | 21 | All | 42.0 | 8.9 |
| SA56(a) | 42.77 | 0.82 | 37 | KL, WE | 44.0 | −1.2 |
| SA56(b) | 53.63 | 1.14 | 20 | WR | 44.0 | 9.6 |
| SA57(a) | 41.94 | 1.02 | 17 | KL | 42.0 | −0.1 |
| SA57(b) | 49.25 | 1.08 | 36 | WE, WR | 42.0 | 7.3 |
| SA59[b] | 50.56 | 1.12 | 19 | All | 45.0 | 5.6 |
| SA60[b] | 54.54 | 1.91 | 17 | All | 45.0 | 9.5 |
| SA61 | 55.16 | 1.88 | 17 | All | 46.0 | 9.2 |
| SA62[b] | 50.94 | 0.59 | 17 | All | 45.0 | 5.9 |
| SA63[b] | 53.48 | 1.14 | 20 | All | 47.0 | 6.5 |
| SA64 | 59.13 | 1.23 | 17 | All | 41.0 | 18.1 |
| SA65 | 56.53 | 0.94 | 20 | All | 45.0 | 11.5 |

Table 2
List of *Pn* wavespeeds estimated for the azimuth ranges in Fig. 7

| Region and azimuth range (Klerksdorp) (°) | Distance range (km) and source region | Intercept (s) | Reciprocal slope (km/s) | Standard deviation (s) | No. of times |
|---|---|---|---|---|---|
| R1 118-233 | 232–555 (KL) | 7.735 ± 0.13 | 8.398 ± 0.023 | 0.38 | 94 |
| | 211–488 (WE) | 7.703 ± 0.16 | 8.389 ± 0.029 | 0.65 | 67 |
| | 265–652 (WR) | 8.272 ± 0.11 | 8.393 ± 0.017 | 0.35 | 119 |
| R2 216-252 | 269–555 (KL) | 7.438 ± 0.27 | 8.340 ± 0.044 | 0.68 | 122 |
| | 211–488 (WE) | 6.943 ± 0.18 | 8.235 ± 0.033 | 0.49 | 133 |
| | 265–652 (WR) | 7.918 ± 0.17 | 8.350 ± 0.024 | 0.47 | 134 |
| R3 233-303 | 200–510 (KL) | 7.367 ± 0.31 | 8.271 ± 0.058 | 0.80 | 104 |
| | 200–471 (WE) | 7.272 ± 0.27 | 8.203 ± 0.056 | 0.69 | 132 |
| | 228–602 (WR) | 7.712 ± 0.20 | 8.275 ± 0.034 | 0.65 | 132 |
| R4 252-338 | 200–492 (KL) | 7.225 ± 0.25 | 8.093 ± 0.052 | 0.57 | 80 |
| | 200–532 (WE) | 8.179 ± 0.22 | 8.272 ± 0.045 | 0.55 | 106 |
| | 205–579 (WR) | 8.729 ± 0.19 | 8.361 ± 0.038 | 0.68 | 152 |
| R5 303-10 | 227–463 (KL) | 8.623 ± 0.19 | 8.304 ± 0.043 | 0.47 | 95 |
| | 232–580 (WE) | 8.894 ± 0.19 | 8.358 ± 0.032 | 0.44 | 108 |
| | 205–473 (WR) | 9.211 ± 0.17 | 8.353 ± 0.036 | 0.40 | 110 |
| R6 338-35 | 227–499 (KL) | 9.382 ± 0.14 | 8.501 ± 0.026 | 0.40 | 125 |
| | 228–603 (WE) | 8.620 ± 0.18 | 8.364 ± 0.027 | 0.57 | 155 |
| | 279–424 (WR) | 8.973 ± 0.33 | 8.313 ± 0.064 | 0.49 | 99 |
| R7 10-83 | 264–553 (KL) | 8.922 ± 0.19 | 8.445 ± 0.031 | 0.41 | 109 |
| | 228–648 (WE) | 8.119 ± 0.15 | 8.323 ± 0.021 | 0.48 | 140 |
| | 230–474 (WR) | 9.621 ± 0.28 | 8.456 ± 0.052 | 0.49 | 93 |
| R8 35-118 | 226–553 (KL) | 7.697 ± 0.28 | 8.282 ± 0.046 | 0.56 | 54 |
| | 251–648 (WE) | 7.411 ± 0.22 | 8.234 ± 0.030 | 0.47 | 69 |
| | 230–474 (WR) | 9.467 ± 0.33 | 8.430 ± 0.061 | 0.50 | 39 |
| R9 83-216 | 226–372 (KL) | 7.908 ± 0.41 | 8.445 ± 0.11 | 0.47 | 43 |
| | 251–468 (WE) | 6.465 ± 0.35 | 8.091 ± 0.060 | 0.43 | 30 |
| | 255–617 (WR) | 8.297 ± 0.24 | 8.359 ± 0.044 | 0.42 | 40 |
| North | 228–553 (KL) | 9.182 ± 0.12 | 8.350 ± 0.024 | 0.47 | 204 |
| | 340–648 (WE) | 9.498 ± 0.15 | 8.485 ± 0.022 | 0.47 | 208 |
| | 205–474 (WR) | 9.293 ± 0.15 | 8.386 ± 0.032 | 0.48 | 205 |
| South | 200–555 (KL) | 7.659 ± 0.16 | 8.357 ± 0.029 | 0.65 | 209 |
| | 201–488 (WE) | 7.998 ± 0.16 | 8.375 ± 0.032 | 0.65 | 262 |
| | 228–652 (WR) | 8.143 ± 0.12 | 8.360 ± 0.020 | 0.46 | 249 |

Approximate mean crustal thicknesses at each station for each source region were estimated from the average crustal thicknesses computed by ray tracing, assuming a crustal thickness of 45 km below each source region. The crustal thickness estimates were then used to estimate systematic differences between the thicknesses of the crust in the three source regions. This was achieved in the following way. If the systematic difference between source regions 1 and 2 is $c_{12}$,

$$c_{12} = \sum_{i=1}^{N} w_{i12}(T_{i1} - T_{i2}) / \sum_{i=1}^{N} w_{i12} \quad (1)$$

where $w_{i12}$ is the number of separate estimates of crustal thickness at station $i$ for source regions 1 and

Fig. 5. Grey-toned contour maps of the estimated crustal thicknesses listed in Table 1. The contour map (a) is for crustal thicknesses inferred from the Pn arrival times and (b) for crustal thicknesses estimated from receiver functions (Nguuri, 2003; Nguuri et al., 2001). Dots represent stations of the SABSE. The hatched area on the insert map indicates the region for which crustal thicknesses were derived, based on *Pn* arrival times. Field of view: 21°; rotation: 0°; tilt: 90°; projection: orthographic.

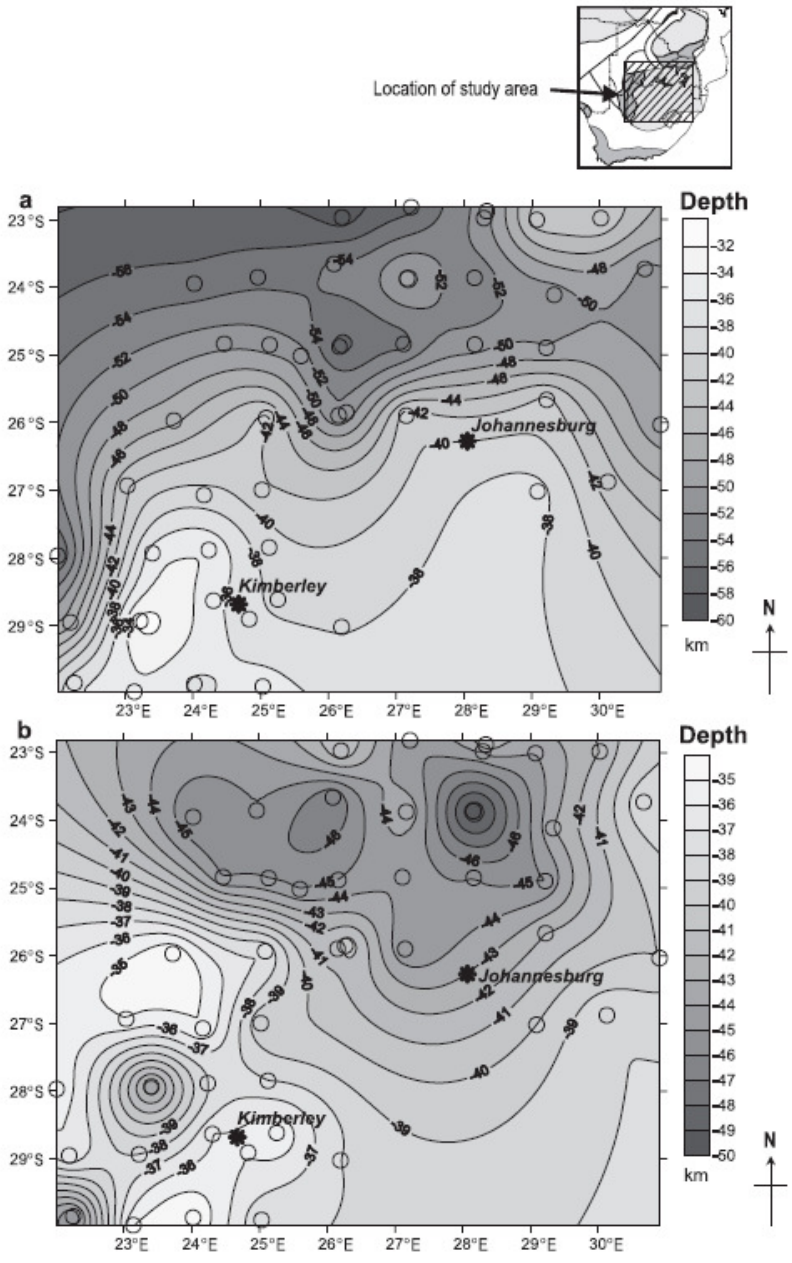
Location of study area
a
b
Depth
km
N
Johannesburg
Kimberley
23°S
24°S
25°S
26°S
27°S
28°S
29°S
23°E
24°E
25°E
26°E
27°E
28°E
29°E
30°E

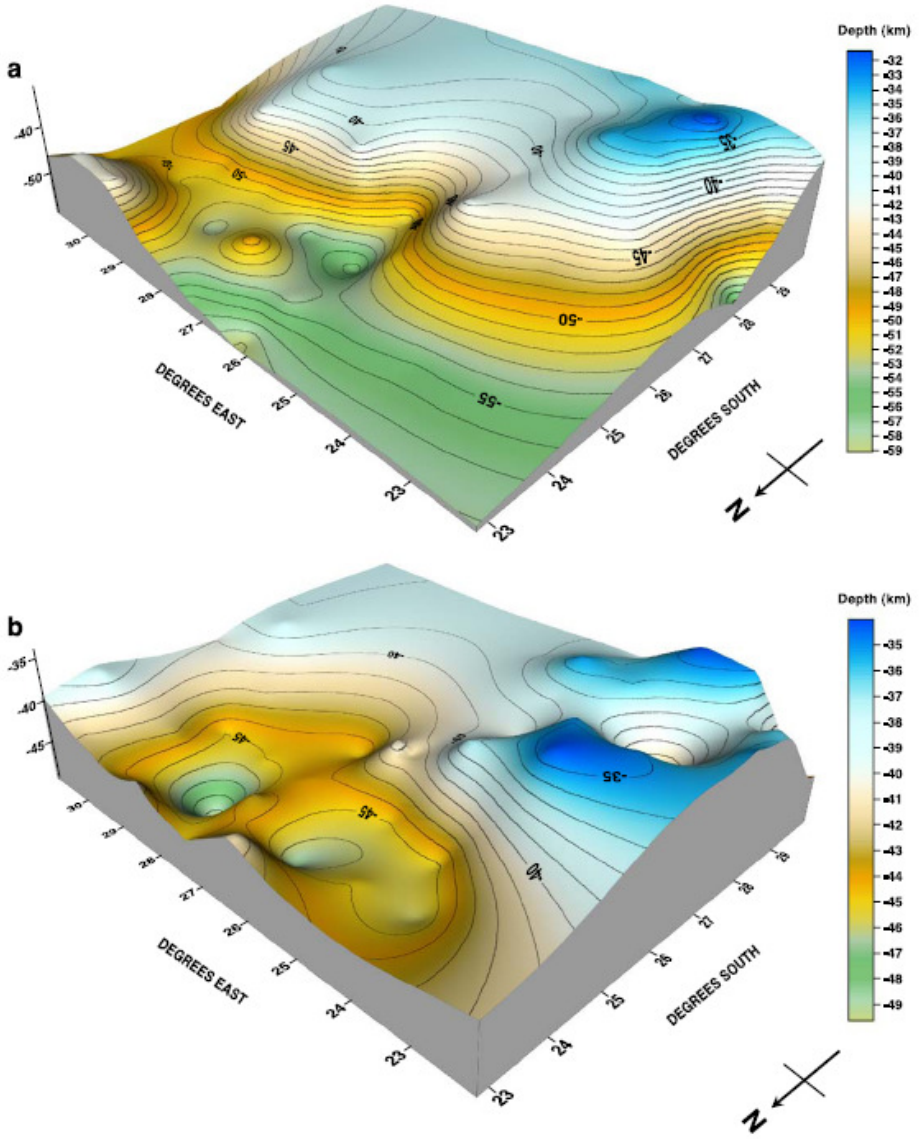


Fig. 6. Perspective plots for (a) crustal thicknesses inferred from the *Pn* arrival times and (b) crustal thicknesses estimated from receiver functions (Nguuri, 2003; Nguuri et al., 2001). Field of view: 45°; rotation: 135°; tilt: 30°; projection: perspective; light position angles: horizontal: 135° and vertical: 45°.

2, and $T_{i1}$ and $T_{i2}$ are the average thicknesses for station $i$ estimated for source regions 1 and 2, respectively. When region 1 is the Far West and West Rand, and 2 is firstly Klerksdorp and secondly Welkom, $c_{12}$ has values of $2.5 \pm 0.30$ km ($N=34$ stations) and $2.2 \pm 0.35$ km ($N=31$ stations), respectively.

Wright et al. (2003) investigated the possibility of bias in event origin times due to errors in the reference P travel–time curve used to refine the origin times. They found a maximum possible bias of 0.46 s (later origin times). When the resulting faster wavespeeds are used to compute crustal thicknesses, there is a shift of 2.0 km to lower thicknesses. In computing the crustal thicknesses listed in Table 1, this maximum correction has been used to make the thicknesses as low as possible to minimize disagreement with earlier seismic studies. To compute crustal thicknesses below each station $i$, the following formulae were used.

$$\text{Far West and West Rand}: \quad H_{\bar{g}1} = 2T_{ij1} - H - 4.0 \tag{2a}$$

$$\text{Klerksdorp}: \quad H_{\bar{g}2} = 2T_{\bar{g}2} - H - 1.5 \tag{2b}$$

$$\text{Welkom}: \quad H_{\bar{g}3} = 2T_{\bar{g}3} - H - 1.8 \tag{2c}$$

where $H_{ijk}$ and $T_{ijk}$ are the estimated crustal thickness below station $i$ and the average crustal thickness (without corrections for origin time bias) for station $i$

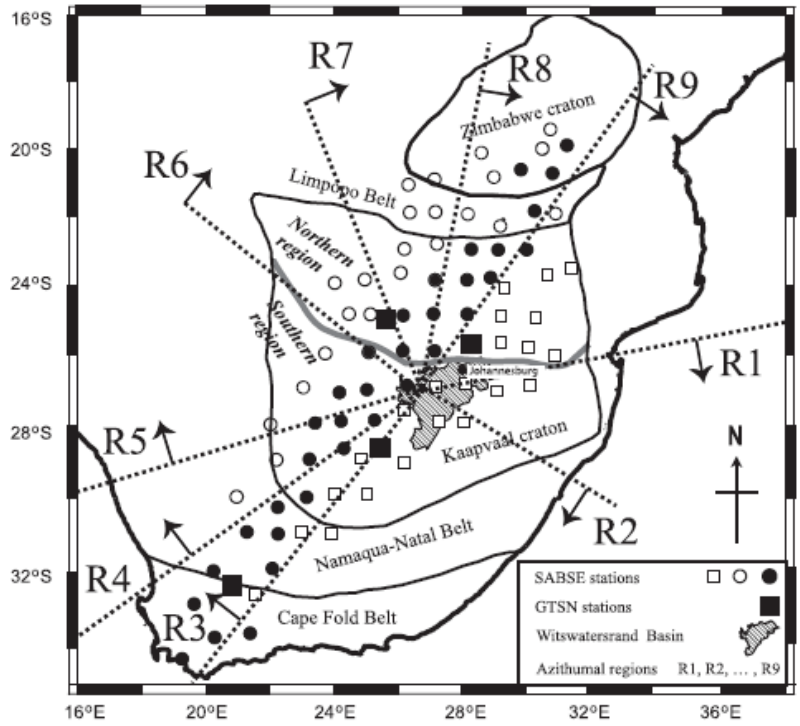


Fig. 7. Map showing subdivision of the Kaapvaal craton region into nine overlapping azimuth ranges for the Klerksdorp region, and division of craton into northern and southern regions. Each azimuth range comprises the segment clockwise from the numbered arrow through the start of the next range to the start of following range. Thus, range 1 covers the region from the line defining the start of range 1 to the line defining the start of range 3, and so on. The subdivisions for the West Rand and Welkom source regions were made as close as possible to those of the Klerksdorp region. Open circles, closed circles and open squares denote SABSE stations that operated from April 1997–April 1998, April 1997–April 1999 and April 1998–April 1999, respectively.

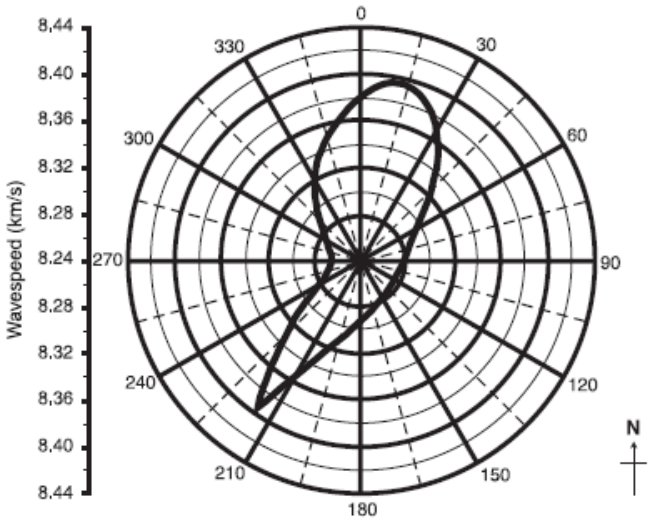


Fig. 8. Polar plot of average wavespeeds for *Pn* arrivals listed in Table 3, using cubic spline smoothing to generate a continuous curve.

and source region *k*, respectively, for event *j* in source region *k*. *H* is the crustal thickness below the Far West and West Rand regions, which has been taken as 43.0 km (the original 45.0 km corrected by 2.0 km to allow for origin time bias). The values of $H_{ijk}$ were averaged for each value of *i*, and are listed together with the thicknesses estimated from receiver functions from Nguuri (2003). The estimates of crustal thicknesses were also calculated from the Ps-P times given by Nguuri (2003) and the P and S wavespeed models of Table 2 of Wright et al. (2003), and were found to be slightly lower than her listed values, but not sufficiently lower to justify using revised values.

Figs. 5 and 6 show grey-toned contour maps and perspective plots of the estimated crustal thicknesses listed in Table 1. The division of the Kaapvaal craton into northern and southern regions is shown in Fig. 7. The average crustal thicknesses for the 19 stations on each of the northern and southern regions of the craton that yielded well-constrained thicknesses were $50.52 \pm 0.88$ km and $38.07 \pm 0.85$ km, respectively. In contrast, the corresponding average thicknesses determined from receiver functions were $43.58 \pm 0.57$ km and $37.58 \pm 0.70$ km, respectively. The contour maps for thicknesses estimated by both methods agree satisfactorily in the southern parts of the craton. The differences are in the northern regions where the refracted arrivals yield greater thicknesses and a steeper, more clearly defined transition between the north and south.

The refracted arrivals also yield anomalously thick estimates of crustal thickness in the southern and western regions. In particular, stations 16 and 22 in the Proterozoic thrust belt just west of the Kheis belt (Fig. 1 and Table 1) yield thicknesses in excess of 45 km, and stations 29 and 37 near the eastern margin of the Kheis belt have thicknesses in excess of 40 km. Receiver functions give clear P-to-S conversions that

Table 3
List of weighted average *Pn* wavespeeds for the azimuth ranges in Fig. 7

| Region | Weighted average seismic P wavespeed (km/s) | Azimuth (°) |
|---|---|---|
| 1 | 8.393 | 215 |
| 2 | 8.315 | 233 |
| 3 | 8.259 | 255 |
| 4 | 8.269 | 290 |
| 5 | 8.344 | 330 |
| 6 | 8.425 | 10 |
| 7 | 8.371 | 40 |
| 8 | 8.275 | 80 |
| 9 | 8.282 | 120 |

imply thicknesses of just 34–36 km for these four stations. The reason for the much larger thicknesses from refracted arrivals is probably a gradual decrease in upper mantle wavespeed to the west, which cannot be resolved without seismic sources west of the Kaapvaal craton. A similar situation occurs with stations 60–61 and 63–65, which lie in the Okwa inlier and the Magondi belt, where the refracted arrivals yield crustal thicknesses 6–18 km greater than those from receiver functions; a decrease in upper mantle wavespeed again seems to be the most plausible explanation. The results thus suggest that the highly depleted uppermost mantle of P wavespeed 8.3–8.4 km extends only as far west as the Kheis belt, and also terminates to the northwest below the Okwa inlier and the Magondi belt.

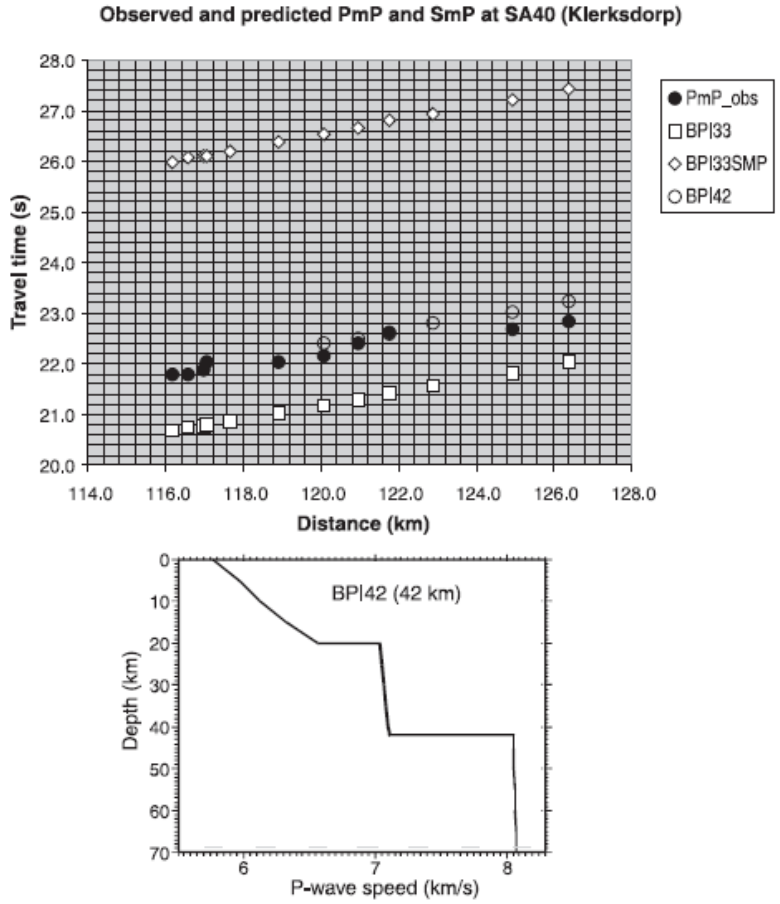


Fig. 9. Travel-time diagram showing observed and predicted *PmP* and predicted *SmP* arrival times at station SA40. The estimated *PmP* arrival times were derived from a source array of ten events in the Klerksdorp mining region. Open diamond symbols indicate theoretical *SmP* times for model BPI33 (P and S, as in Table 2 of Wright et al., 2003), open squares predicted *PmP* times for model BPI33, and open circles predicted *PmP* times for model BPI42. Solid circles denote observed *PmP* arrivals, which indicate a crustal thickness of about 42 km. BPI33 and BPI42 denote models with crusts 33 and 42 km thick, respectively. The insert is a graphical presentation of P model BPI42.

In Table 1, *Pn* arrivals at station 38 to the north and west of the seismic sources suggest a crustal thickness some 12 km greater for paths from Welkom than for the other two source regions, and similar results are found for *Sn* arrivals. This suggests that paths from the Far West and West Rand, and Klerksdorp regions miss the underplated mafic lower crust whose boundary is defined approximately in Fig. 7 (Wright et al., 2003). Even more intriguing are the results for stations 51, 56 and 57, which lie in similar azimuths from the source regions, and give ambiguous crustal thicknesses that vary by 7–11 km between different source regions. This effect may be caused by gaps or 'thin zones' in the underplated region, so that there are 'fast paths' from sources in the southern part of the craton to some stations situated in the underplated region. Wright et al. (2003) explain the differences in estimates of crustal thickness from receiver functions and refracted arrivals in the northern Kaapvaal craton as being due to the variable S wavespeed contrasts between mantle peridotites and mafic granulites (base of lower crust) and mafic and intermediate granulites (top of lower crust). This effect arises because the seismic properties of mafic rocks in the deep crust can vary quite significantly with relatively small changes in composition and metamorphic grade (Hurich et al., 2001), making it difficult to define the petrological crust–mantle boundary using receiver functions.

## 5. Azimuthal variations in seismic wavespeed in the upper mantle and possible anisotropy

The average P wavespeeds in the uppermost mantle were found to be almost the same in the northern and southern regions of the Kaapvaal craton, with the suggestion of slightly higher values for the northern region. To determine if regional variations in *Pn* wavespeed were detectable, either as a consequence of real variations in the upper mantle or systematic changes in crustal properties as a function of source-to-station distance, the time data were divided into nine overlapping azimuth ranges, as shown in Fig. 7 for Klerksdorp. The subdivisions for the Far West and West Rand and Welkom regions were made as close as possible to those of Fig. 7, and the results of the regression line fits are shown in Table 2.

To test for evidence of pervasive azimuthal anisotropy across the entire craton, the weighted average reciprocal slopes of Table 1 were calculated for each of the nine regions, and plotted against an approximate average azimuth for each region (Fig. 8 and Table 3). Despite the crudeness of the analysis and the non-uniform distribution of data with respect to both azimuth and distance, there are maxima in seismic wavespeed at azimuths of about 15° and 217°, and, although data to the east are sparse, the suggestion of minima at azimuths of roughly 90° and 270°. Fig. 8 clearly suggests coherent azimuthal anisotropy across the entire craton, with the wavespeed maximum of about 8.40 km/s slightly east of north, and a minimum of about 8.25 km/s. The distortion of the azimuthal distribution of wavespeeds is due to very poor coverage from northeast to south. We cannot be sure that we are measuring azimuthal anisotropy because the wavespeeds are measured radially outwards from the three source regions like the spokes of a wheel, and comparison with other evidence for anisotropy is essential. Vinnik et al. (1996) and Silver et al. (2001) inferred a fast polarization direction in the NE–SW direction from their studies of shear-wave splitting in the mantle of the Kaapvaal craton using SKS phases, which follows the trend of Archaean structures, with the most anisotropic regions being Archaean in age. Silver et al. (2001) concluded that Archaean mantle deformation to depths of greater than 200 km is preserved as fossil mantle anisotropy. The present results correlate satisfactorily with the results of shear-wave splitting, suggesting that the uppermost mantle sampled by the *Pn* arrivals has preserved the same history of mantle deformation. They are also consistent with the inference of Schulte-

Fig. 10. Vertical-component seismograms plotted as reduced times for two events from the Klerksdorp mining region recorded by stations to the north and west of the source (Figs. 1 and 7). The reduction velocity for these plots is 8.2 km/s, with time in seconds relative to the respective origin times of the earthquakes. The original seismograms were bandpass-filtered between 2.0 and 7.0 Hz. Amplitudes were automatically scaled by the SAC program (Tapley and Tull, 1992). The solid horizontal bars at the base of the traces indicate the times of the first P arrivals. Arrows indicate a region of anticipated change of structure across the Limpopo belt (Fig. 1). Epicentral parameters of events in a and b, respectively, are: July 21, 1997, 26.8962° S and 26.7793° E, depth 0.72 km, origin time 08:45:50.2 UT, $M_L$=4.0; January 17, 1998, 26.8824° S and 26.7798° E, depth 0.62 km, origin time 13:06:45.1 UT, $M_L$=3.8.

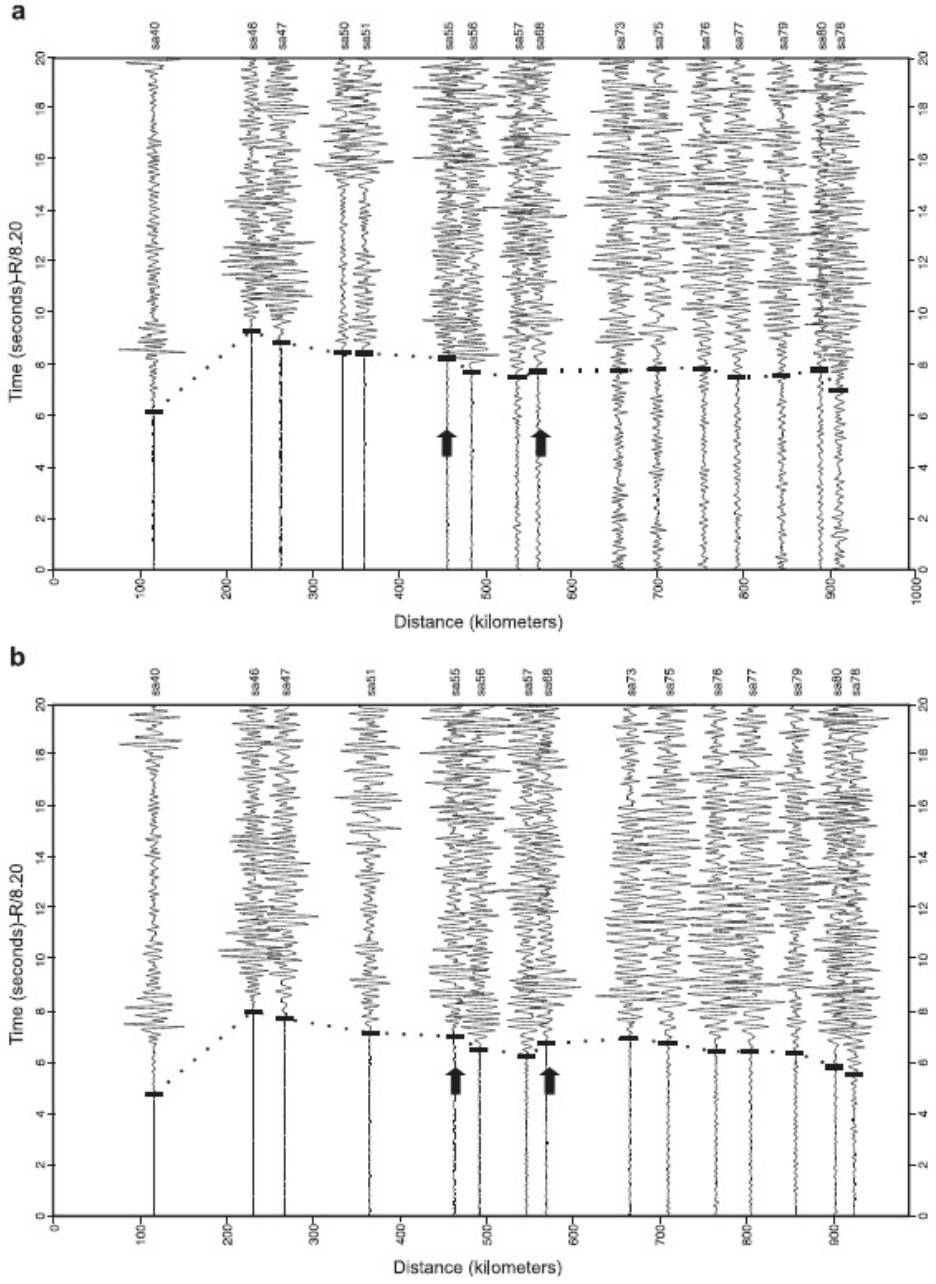
a
ss40
ss46
ss47
ss50
ss51
ss55
ss56
ss57
ss68
ss73
ss75
ss76
ss77
ss79
ss80
ss78
Time (seconds)-R/8.20
Distance (kilometers)
b
ss40
ss46
ss47
ss51
ss55
ss56
ss57
ss68
ss73
ss75
ss76
ss77
ss79
ss80
ss78
Time (seconds)-R/8.20
Distance (kilometers)

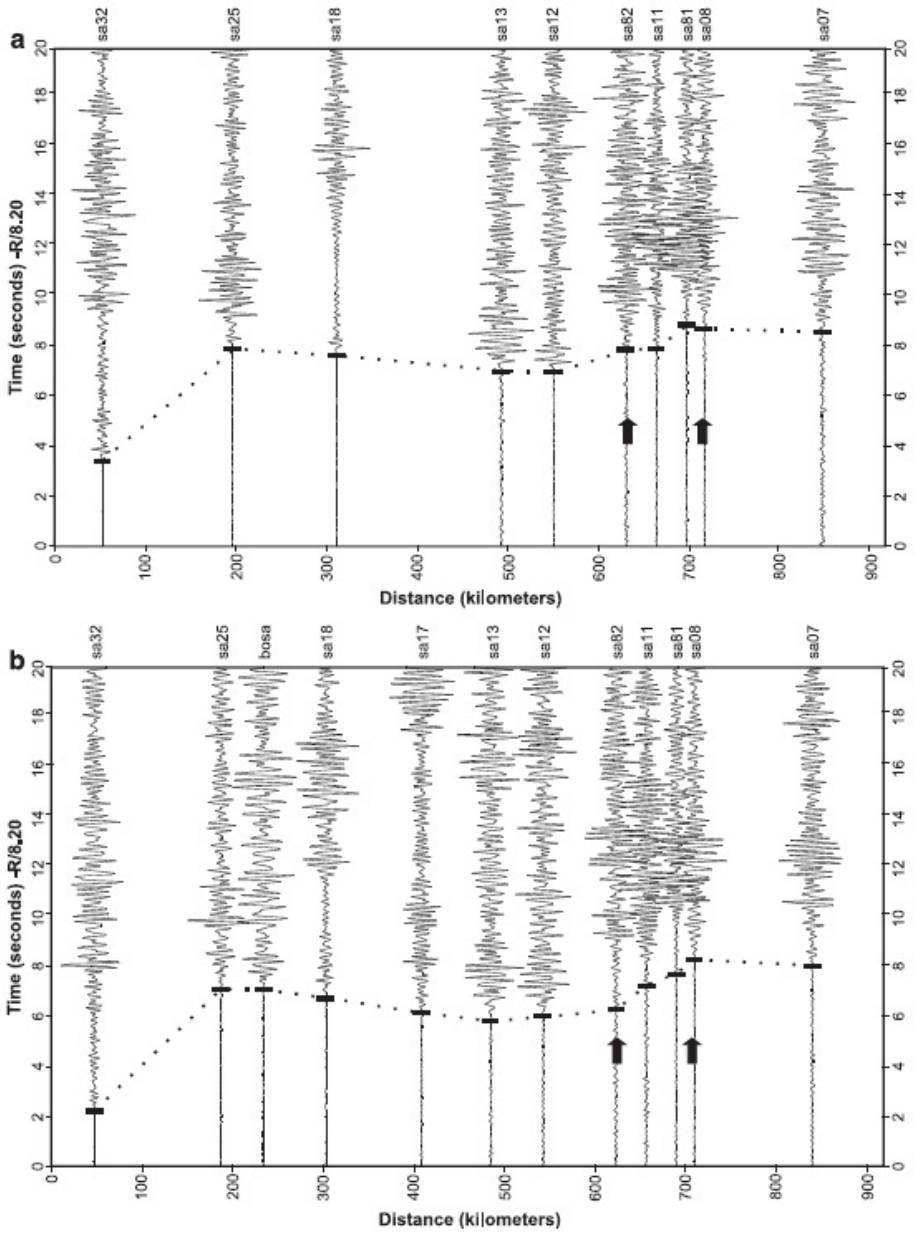
a
sa32
sa25
sa18
sa13
sa12
sa82
sa11
sa81
sa08
sa07
Time (seconds) -R/8.20
Distance (kilometers)
b
sa32
sa25
bosa
sa18
sa17
sa13
sa12
sa82
sa11
sa81
sa08
sa07
Time (seconds) -R/8.20
Distance (kilometers)

Pelkum et al. (2001) that the fast directions on cratons inferred by P wave polarization, *Pn* travel times and SKS splitting are aligned with absolute plate motions.

## 6. *PmP* phases and seismic records

The *PmP* phase, which is a wide-angle reflection from the Moho, can have large amplitudes, but the onsets are often emergent, making its use to estimate reliable crustal thicknesses difficult (Wright et al., 2003). A few examples of *PmP* phases have been obtained at distances less than 200 km using source arrays (accurately located earthquakes clustered within an area of a few hundred square kilometres). Fig. 9 shows *PmP* arrival times at station 40 (Fig. 1) from a source array of 10 events in the Klerksdorp mining region at distances between 116 and 126 km, together with computed *PmP* and *SmP* travel times for different crustal thicknesses. A crustal thickness of 42 km provides a good fit to the data for a location half way between Klerksdorp and station 40. This value appears reasonable when compared with the estimates of crustal thickness at station 40 (41 km from refracted arrivals and 45 km from receiver functions (Table 1)).

Figs. 10 and 11 are vertical-component records for two different events from the Klerksdorp region, recorded at stations to the northern (Fig. 10) and southern (Fig. 11) regions of Fig. 7. In Fig 10, arrows at stations 55 and 68 (Fig. 1) mark locations at the southern and northern margins of the Limpopo belt, respectively, beyond which there is an offset from the linear trend of reduced times to significantly later times at distances of 560 km onwards, where all stations lie within the northern marginal zone of the Limpopo belt or within the Zimbabwe craton. Fig. 10 shows how reproducible the travel time anomalies are for nearby seismic events, and illustrates the likelihood of both changes in crustal thickness and mantle wavespeeds that make the method of estimating crustal thicknesses applicable only to the northern Kaapvaal craton and the southern marginal zone of the Limpopo belt. Fig. 11 shows much larger time delays beyond station 12, which is just off the southern margin of the Kaapvaal craton. The late arrival times at stations within the Namaqua-Natal belt suggest both lateral reductions in mantle wavespeed and the increases in crustal thickness that are confirmed by the receiver functions (Nguuri et al., 2001). However, the presence of a low wavespeed zone within the upper mantle as well as an increase in crustal thickness (Wright et al., 2003) is an alternative explanation.

## 7. Conclusions

*Pn* arrivals from mining-induced tremors recorded at stations of the SABSE indicate that the seismic wavespeeds in the uppermost mantle of the Kaapvaal craton are relatively uniform and generally lie between 8.3 and 8.4 km/s, indicating the presence of highly depleted Mg-rich peridotites. This comparative uniformity of wavespeed allows use of a simple method of estimating crustal thicknesses for seismic stations on the craton. The estimated crustal thicknesses within the southern part of the craton vary between 31 and 56 km, with an average of $38.07 \pm 0.85$ km for the 19 most centrally located stations. This average compares well with the average of $37.58 \pm 0.70$ km estimated from receiver functions for the same stations. Anomalously high estimates of crustal thicknesses from refracted arrivals compared with corresponding results for receiver functions occur in the western part of the craton, and are attributed to a decrease in upper mantle P wavespeed towards the west. The *Pn* arrivals indicate crustal thicknesses in the northern part of the craton that lie between 41 and 59 km, and an average crustal thickness of $50.52 \pm 0.88$ km for the 19 most centrally located stations: some 7 km greater than the

Fig. 11. Vertical-component seismograms plotted as reduced times for two events from the Klerksdorp mining region recorded by stations to the south and west of the source (Figs. 1 and 7). The reduction velocity for these plots is 8.2 km/s, with time in seconds relative to the respective origin times of the earthquakes. The original seismograms were bandpass-filtered between 2.0 and 7.0 Hz. Amplitudes were automatically scaled by the SAC program (Tapley and Tull, 1992). The solid horizontal bars at the base of the traces indicate the times of the first P arrivals. Arrows indicate a region of rapid change of structure in the northern part of the Namaqua-Natal belt (Fig. 1). Epicentral parameters of events in a and b, respectively, are: July 21, 1997, 26.8962 °S and 26.7793 °E, depth 0.72 km, origin time 08:45:50.2 UT, $M_L = 4.0$; December 12, 1997, 26.6640 °S and 26.7481 °E, depth 0.63 km, origin time 16:42:47.3 UT, $M_L = 4.3$.

corresponding average thicknesses determined from receiver functions (43.58 ± 0.57 km). This difference is attributed to the variable seismic properties of mafic granulites in the underplated northern part of the craton, which results in lack of a clearly defined Moho in the receiver functions. Furthermore, the transition between the northern and southern regions is much more clearly defined by the *Pn* arrivals than by receiver functions. For some directions from sources in the Witwatersrand basin to stations in the northern region, estimates of crustal thickness are bimodal and are attributed to the availability of paths through the mantle that narrowly miss the incompletely underplated northern region. In the northern region of the craton, crustal thicknesses are probably slightly underestimated from both receiver functions and *Pn* arrivals because the P and S wavespeeds in the lower crust used in the calculations are too low for mafic granulites.

There is a detectable dependence of *Pn* wavespeed on source-to-station azimuth which may indicate a small but pervasive azimuthal anisotropy throughout the Kaapvaal craton, in which the maximum wavespeeds are at azimuths of about 15° and 217° in the northern and southern regions of the craton, respectively. Such anisotropy would result in slight underestimates and overestimates, respectively, of crustal thicknesses at stations situated on fast and slow source-to-station azimuths, respectively.

## Acknowledgements

Financial support for the running of the Southern African Broadband Seismic Experiment (SABSE) was provided by the National Research Foundation (South Africa), the National Science Foundation (USA), the University of the Witwatersrand Research Council, the Department of Geological Survey (Botswana), the University of Botswana and several southern African mining companies. M.T.O.G. Kwadiba received financial support from the Government of Botswana, the Kellogg Foundation and the University of the Witwatersrand, E.M. Kgaswane from the National Research Foundation and the Council for Geoscience, R.E. Simon from the University of Botswana, and T.K. Nguuri from the Mellon Foundation. Assistance provided by staff of the Carnegie Institution of Washington (USA) and members of the Kaapvaal Research Group is gratefully acknowledged. David E. James offered helpful suggestions and valuable advice, for which we are grateful. We are also most grateful to Fenglin Niu and Derek Schutt for providing numerous UNIX scripts that were used in the processing of data.

## References

Andreoli, M.A.G., Doucouré, M., Van Bever Donker, J., Brandt, D., Andersen, N.J.B., 1996. Neotectonics of southern Africa—a review. Afr. Geo. Rev. 3, 1–16.

Baumont, D., Paul, A., Zandt, G., Beck, S.L., 2001. Inversion of *Pn* travel times for lateral variations of Moho geometry beneath the Central Andes and comparison with the receiver functions. Geophys. Res. Lett. 28, 1663–1666.

Boyd, F.R., Gurney, J.J., 1986. Diamonds and the African lithosphere. Science 232, 472–477.

Boyd, F.R., Gurney, J.J., Richardson, S.H., 1985. Evidence for a 150–200 km thick Archean lithosphere from diamond inclusion thermobarometry. Nature 315, 387–389.

Carlson, R.W., Grove, T.L., de Wit, M.J., Gurney, J.J., 1996. Program to study crust and mantle of the Archean craton in southern Africa. EOS 77 (29), 273 and 277.

De Wit, M.J., Roering, C., Hart, R.J., Armstrong, R.A., Ronde, C.E.J., Green, R.W.E., Tredoux, M., Peberdy, E., Hart, R.A., 1992. Formation of an Archaean continent. Nature 357, 553–562.

Graham, G. (Ed.), 1997. Seismological Bulletins (produced monthly). Council for Geoscience, Pretoria, South Africa, April–December issues.

Graham, G. (Ed.), 1998. Seismological Bulletins (produced quarterly). Council for Geoscience, Pretoria, South Africa, January–March, April–June, July–September and October–December issues.

Graham, G. (Ed.), 1999. Seismological Bulletins (produced quarterly). Council for Geoscience, Pretoria, South Africa, January–March and April–June issues.

Hofmann, A.W., 1988. Chemical differentiation of the earth: the relationship between mantle, continental crust, and oceanic crust. Earth Planet. Sci. Lett. 90, 297–314.

Hurich, C.A., Deemer, S.J., Indares, A., 2001. Compositional and metamorphic controls on velocity and reflectivity in the continental crust: an example from the Grenville Province of eastern Québec. J. Geophys. Res. 106, 665–682.

Ireland, T.R., Rudnick, R.L., Spetsius, Z., 1994. Trace elements in diamond inclusions from eclogites reveal link to Archaean granites. Earth Planet. Sci. Lett. 128, 199–213.

Kgaswane, E.M., Wright, C., Kwadiba, M.T.O., Webb, S.J., McRae-Samuel, R., 2002. A new look at South African seismicity using a temporary network of seismometers. S. Afr. J. Sci. 98, 377–384.

Kulhanek, O., Meyer, K., 1979. A proposal for a seismograph station network in Ngamiland, Botswana. Seismological Institute, Uppsala, Sweden.

Mason, R., 1973. The Limpopo mobile belt-southern Africa. Phil. Trans. R. Soc. London, Series A 273, 463–485.

Nguuri, T.K., 2003. Crustal structure of the Kaapvaal craton and surrounding mobile belts: analysis of teleseismic P waveforms and surface wave inversions. PhD thesis, the University of the Witwatersrand, Johannesburg.

Nguuri, T.K., Gore, J., James, D.E., Webb, S.J., Wright, C., Zengeni, T.G., Gwavava, O., Snoke, J.A., The Kaapvaal Seismic Group, 2001. Crustal structure beneath southern Africa and its implications for the formation and evolution of the Kaapvaal and Zimbabwe cratons. Geophys. Res. Lett. 28, 2501–2504.

Pretorius, D.A., 1986. The Witwatersrand Basin: Surface and Subsurface Geology and Structure. Economic Geology Research Unit, University of the Witwatersrand, Johannesburg, South Africa.

Rudnick, R.L., 1995. Making continental crust. Nature 378, 571–577.

Schulte-Pelkum, V., Masters, G., Shearer, P.M., 2001. Upper mantle anisotropy from long-period P polarization. J. Geophys. Res. 106, 21917–21934.

Shearer, P.M., Oppenheimer, D.H., 1982. A dipping Moho and crustal-velocity zone from *Pn* arrivals at the Geysers-Clear Lake, California. Bull. Seismol. Soc. Am. 72, 1551–1566.

Silver, P.G., Gao, S.S., Liu, K.H., the Kaapvaal Seismic Group, 2001. Mantle deformation beneath southern Africa. Geophys. Res. Lett. 28, 2493–2496.

Tapley, W.C., Tull, J.E., 1992. SAC-Seismic Analysis Code, Users Manual, Revision 4. Lawrence Livermore National Laboratory, Livermore, CA. 278 pp.

Van Zijl, J.S.V., 1978. The relationship between the deep electrical resistivity structure and tectonic provinces in southern Africa. Part I. Results obtained by Schlumberger soundings. Trans. Geol. Soc. Afr. 81, 129–142.

Vetter, U., Minster, J.B., 1981. *Pn* velocity anisotropy in southern California. Bull. Seismol. Soc. Am. 71, 1511–1530.

Vinnik, L.P., Green, R.W.E., Nicolaysen, L.O., 1996. Seismic constraints on dynamics of the mantle of the Kaapvaal craton. Phys. Earth Planet. Inter. 95, 139–151.

Wright, C., Fernandez, L.M., 2003. Earthquakes, seismic hazard and earth structure in South Africa (national report for South Africa). In: Lee, W.H.K., Kanamori, H., Jennings, P.C., Kisslinger, C. (Eds.), International Handbook of Earthquake and Engineering Seismology, Part B, International Association of Seismology and the Physics of the Earth's Interior (I.A.S.P.E.I.). Elsevier, Amsterdam.

Wright, C., Kwadiba, M.T.O., Kgaswane, E.M., Simon, R.E., 2002. The structure of the crust and uppermantle to depths of 320 km beneath the Kaapvaal craton, from P wave arrivals generated by regional earthquakes and mining-induced tremors. J. Afr. Earth Sci. 35, 477–488.

Wright, C., Kgaswane, E.M., Kwadiba, M.T.O., Simon, R.E., Nguuri, T.K., McRae-Samuel, R., 2003. South African seismicity, April 1997–April 1999, and regional variations in the composition of the crust and uppermost mantle. Lithos 71, 369–392 (this issue).

Zervas, C., Crosson, R.S., 1986. *Pn* observation and interpretation in Washington. Bull. Seismol. Soc. Am. 76, 521–546.